K. Jantschik, O. Czaikowski, H. C. Moog and *K. Wieczorek*

Investigating the sealing capacity of a seal system in rock salt (DOPAS project)

This paper describes research and development work on plugging and sealing repositories, an issue of fundamental importance for the rock salt option which represents one of the three European repository options, besides the clay rock and the crystalline rock options. The programme aims at providing experimental data needed for the theoretical analysis of the long-term sealing capacity of concrete-based sealing materials. In order to demonstrate hydro-mechanical material stability under representative load scenarios, a comprehensive laboratory testing programme is carried out. This comprises investigation of the sealing capacity of the combined seal system and impact of the so-called excavation-damaged zones (EDZ) as well as investigation of the hydro-chemical long-term stability of the seal in contact with different brines under diffusive and advective conditions. This paper presents experimental approaches and preliminary results from laboratory investigations on salt concrete and combined systems as obtained to date.

Untersuchung des Abdichtungsvermögens eines Verschlusssystems im Steinsalz. *Im nachfolgenden Paper werden ausgewählte FuE-Arbeiten für Verschlusssysteme von Endlagern für wärmeentwickelnde hochradioaktive Abfälle im Steinsalz dargestellt. Steinsalz stellt – neben Ton- und Kristallingestein – eine der drei Endlageroptionen in Europa dar. Im Rahmen der Forschungsarbeiten werden anhand von Laborversuchen experimentelle Daten für die theoretische Analyse des Langzeitdichtvermögens von zementbasierten Dichtbaustoffen ermittelt. Hierzu wird ein umfangreiches Versuchsprogramm durchgeführt, um sowohl die hydro-mechanische als auch die hydro-chemische Materialbeständigkeit zementbasierter Dichtbaustoffe zu ermitteln. Dazu werden sowohl kombinierte Verschlusssysteme und die Einwirkung auf die Auflockerungszone (EDZ) untersucht als auch die hydraulisch-chemische Langzeitstabilität unter diffusiven und advektiven Bedingungen in Kontakt zu verschiedenen Lösungen. Nachfolgend werden bislang durchgeführte Experimente und deren vorläufige Ergebnisse an Salz- und Sorelbetonprüfkörpern sowie an kombinierten Systemen vorgestellt.*

1 Introduction

The German safety requirements for a repository of heat-generating nuclear waste [1] comprise several safety principles. The most important ones are:

- Radionuclides and other contaminants in the waste must be concentrated and contained in a containment-providing rock zone and thus be isolated from the biosphere as long as possible.
- Waste disposal must ensure that release of radionuclides from the repository enhances only insignificantly the risks resulting from natural radiation exposure.

Besides the geological barrier, backfill and seal systems are required to ensure that the safety principles are met. On behalf of the Federal Ministry for Economic Affairs and Energy (BMWi), the national funding organisation for R&D work related to radioactive waste management in Germany, GRS is investigating sealing and backfilling materials potentially utilised in salt and clay formations. The programme aims at providing experimental data needed for the theoretical analysis of the long-term sealing capacity of these sealing materials and is related to two large-scale projects:

- The DOPAS Full-Scale Demonstration of Plugs and Seals project performed by 14 beneficiaries from 8 European countries focuses on demonstration activities in plugging and sealing. These activities are also a part of each participant's national long-term R&D programmes and are therefore jointly funded by Euratom's 7th Framework Programme and by national funding organisations. The demonstration experiments will be partially or entirely implemented during the DOPAS project lifetime from 2012 to 2016 [2].
- ELSA is a national project of laboratory and in-situ experiments that aims at further developing the reference shaft seal for the German disposal concept for a repository in rock salt and at developing reference shaft seals for a repository in clay host rocks [3].

2 Seal systems in rock salt

In repository concepts for the disposal of nuclear waste in rock salt formations, the salt host rock is the primary barrier ensuring permanent waste containment. The salt rock is characterized by a very low porosity, a low permeability, a low water content and its pronounced visco-plastic deformation behaviour which causes the closure of voids with time under compressive stress states.

According to the current concept in Germany, crushed salt is used to backfill the mine openings. With time it is compacted by convergence to low porosity and permeability and takes an important sealing function in the long term, when a sufficiently high hydraulic resistance to avoid entry of brine into the emplacement areas of the repository is achieved.

In the early post closure phase of a repository, the sealing capability of the backfill is, however, low. During this time, sealing of the backfilled openings has to be provided by geotechnical barriers, like borehole plugs and drift seals. These have the task to preserve the integrity of the geological barrier, to stabilize the disturbed rock zone at the contour and to limit and decelerate the inflow of brine.

During and after construction of an excavation, stress redistribution and dilation of the salt close to the opening leads to micro-fracturing and pore volume increase (dilatancy). The EDZ can exhibit a permeability which is several orders of magnitude higher than the undisturbed rock. For increasing the effectiveness of seal systems, most of the EDZ will be removed prior to seal emplacement. When investigating sealing effectiveness, the combined system of the seal itself, the contact area, and the residual part of the EDZ has to be considered [4].

In order to fulfil their purpose, the materials used for plugging and sealing as well as the complete seal system must have a sufficiently low permeability under the prevailing hydro-mechanical conditions, as sketched in Fig. 1. Moreover, they have to be stable against corrosion in the presence of brine in the short and long term.

According to recent R&D work on the salt option, materials for shaft and drift seal components currently considered in Germany comprise MgO and cement-based salt concrete [5].

In order to demonstrate hydro-mechanical material stability under representative load scenarios, a comprehensive laboratory testing programme is carried out. This comprises investigation of the sealing capacity of the combined seal system and impact of the EDZ as well as investigation of the hydro-chemical long-term stability of the seal in contact with different brines under diffusive and advective conditions, with the focus on salt concrete systems.

This paper presents experimental approaches and preliminary results from laboratory investigations on salt concrete and combined systems as obtained to date. The experiments will be used as a basis for simulation/improvement cycles to advance model validation and calibration.

3 Experimental investigations

The experimental investigations concentrate on salt concrete as a candidate drift seal material and on combined salt concrete/rock salt systems, as the sealing function is affected by the salt concrete itself, the contact zone between concrete and host rock and the excavation damaged zone close to the seal (Fig. 2).

Samples for experimental investigations were drilled from an in-situ construction in a former salt mine. The drift sealing element had been constructed at the 945 m level of the mine in January 1992. Its dimensions were 8.0 m in length, 5.5 m in width and 3.4 m in height. The samples were taken from two boreholes (B4 and B5, see Fig. 2). The salt concrete is a mass concrete consisting of a cement matrix with crushed salt filler. The composition is given in Table 1. At the time of sampling the seal had been subjected to convergence of the surrounding rock salt for about ten years. Figure 3 shows some of the samples before testing.

The following laboratory tests have been performed or are in planning:

- Triaxial tests on salt concrete for investigating mechanical stability,
- Uniaxial tests to determine salt concrete long-term deformation behaviour,
- hydro-mechanical investigations of the combined system of salt concrete/rock salt and
- investigation of long-term chemical stability of the combined system of salt concrete/rock salt.

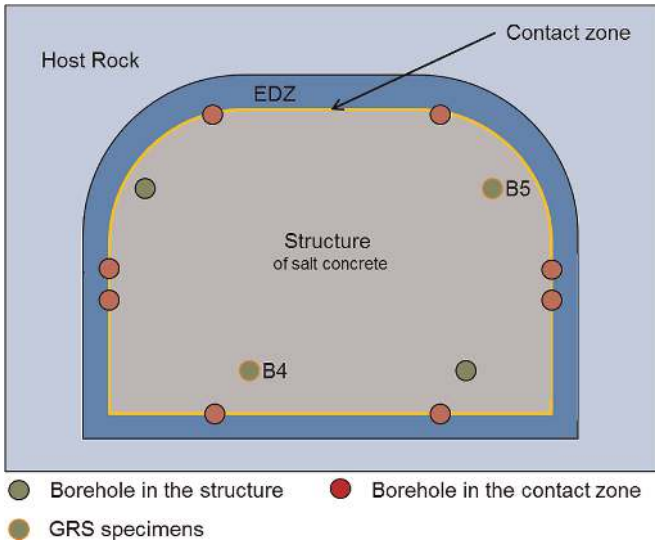

Fig. 2. Definition of the three parts of a sealing system and identification of the sample boreholes [11]

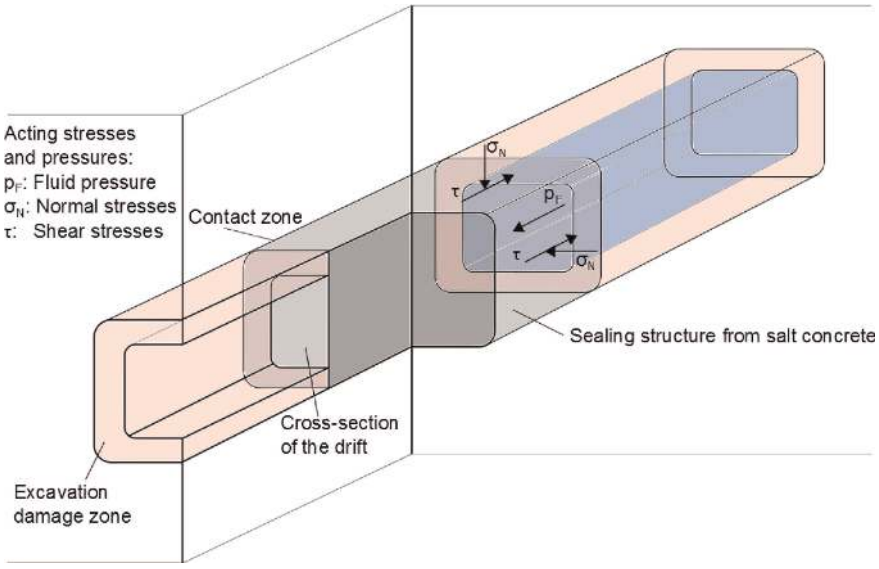

Fig. 1. Sketch of a drift seal system with acting stresses [10]

Table 1. Composition of salt concrete [11]

Component of salt concrete	Proportion in [kg/m^3]	Proportion in mass-%
Blast furnace cement	380	18.3
Crushed salt	1.496	72.1
NaCl-brine	198	9.5
Total	2.074	100.0

Fig. 3. Salt concrete samples before testing

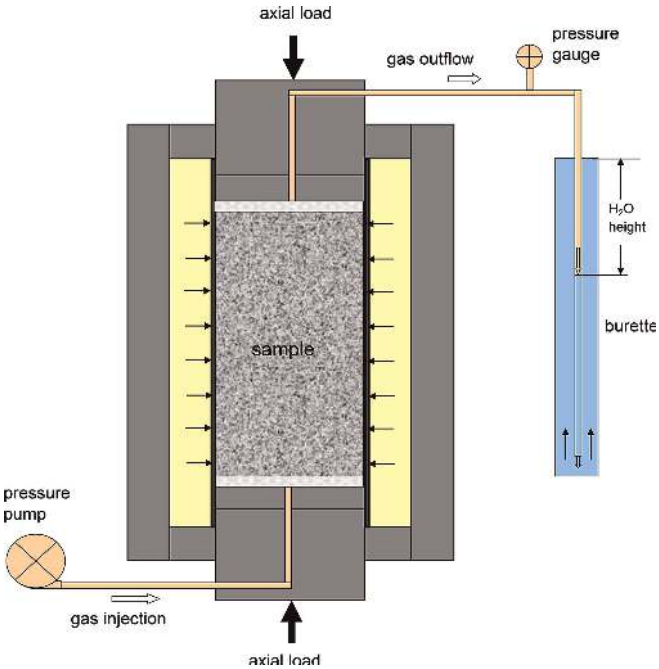

Fig. 4. Principle of triaxial compression tests with permeability measurement

3.1 Salt concrete stability

Triaxial compression tests (TC-Tests) were performed in order to investigate the mechanical stability of salt concrete. Onset of dilatancy, start of gas flux and failure of the specimens were determined under different radial stresses. The results of the TC-Tests aim at a better understanding of the difference in deformation behaviour of salt concrete with respect to uniaxial creep testing.

3.1.1 Experimental layout and testing procedure

Damage tests were carried out on 3 salt concrete samples in a triaxial apparatus and deformation and gas permeabilities were measured under various stress conditions. The samples are shown in Fig. 3. Open voids stemming from the hydration process marked in red on the samples were filled with resin during the sample preparation procedure. The average porosity of the samples was about $\Phi = 6\,\%$ with a grain density 2.17–2.2 g/cm^3. The average water content was at a level of w = 2 weight-%.

Figure 4 illustrates schematically the assembly of a sample in a triaxial cell. The sample was isolated in a jacket and porous discs at top and bottom. The samples were subjected to two phases with different loading regimes. The purpose of the initial isostatic pre-compaction phase was to re-establish the intact state of the samples with respect to permeability. It has to be pointed out, though, that no effective healing was expected during the pre-compaction phase. This phase was performed by simultaneously increasing axial and radial stress to $\sigma_a = \sigma_r = 5$ MPa at a loading rate of 1 MPa/min, then keeping stress constant for 22 hours. Then, the axial and radial stresses were increased twice up to a level of 20 MPa. After 24 hours, the pre-compaction phase ended. The idea of this pre-compaction phase is to reach the state of compaction that the specimens had before extraction from the drift sealing element.

In the second step of the test the specimens were deformed under deviatoric stress. For that purpose, three specimens were subjected to three confining stresses of 1, 2 and 3 MPa. The axial stress was increased until the failure load level of the sample was reached. A low strain rate of $\dot{\varepsilon}_a = 1 \cdot 10^{-7}\ s^{-1}$ was applied.

During the load tests, axial strain was measured by a displacement-transducer installed outside of the cell, while volumetric strain was determined both directly from the volume change of the confining oil in the cell by using a pressure/volume controller and indirectly by strain gauges attached on the sample surface at the middle of the length.

Permeability changes induced by the mechanical loading were measured along the sample axis by injecting dry nitrogen gas to the bottom at constant pressure and recording the outflow at the opposite side. The gas outflow was continuously recorded by using a burette. During steady state gas flow, the permeability is determined according to Darcy's law for compressive media:

$$k = \frac{2 \cdot Q \cdot \mu \cdot L \cdot p_o}{A \cdot (p_g^2 - p_o^2)} \qquad (1)$$

where k is the intrinsic permeability (m^2), Q is the flow rate of the gas (m^3/s), μ is the gas dynamic viscosity (Pa · s), L is the length of the sample (m), A is the cross section of the sample (m^2), p_o is the atmospheric pressure (Pa), p_g is the gas injection pressure (Pa). The measuring system allows a precise determination of low permeabilities down to $\sim 10^{-21}$ m^2.

3.1.2 Test results and interpretation

The results of the TC-Tests with a confining stress of 3 MPa are presented in Fig. 5 and Fig. 6. In Fig. 5, the deviatoric stress and the volumetric strain are shown versus the axial strain. The deviatoric stress increases up to a stress level of

40 MPa. The failure stress is reached at an axial strain of 2 %. After failure, gas permeability measurements are performed (Fig. 6). Axial deformation is kept constant during the measurement. Hence, stresses show relaxation behaviour during the gas permeability measurements. Afterwards, axial stress is increased further. The volumetric strain decreases in the beginning of the test, due to the compaction of the specimen. Volumetric strain starts to increase when axial strain reaches values of about 0.9 %. This point is defined as the onset of dilatancy, which is marked by formation of microcracks leading to volume increase. At this point, the deviatoric stress is about 36 MPa. By ongoing increase of deviatoric stress the microcracking and the specimen volume increases further. At a certain point of the test the microcracks are connected and a gas flow can be detected (Fig. 6).

The results of the triaxial compression tests show that salt concrete exhibits reversible (elastic) and irreversible (plastic) material behaviour during the compaction phase. The compaction test phase was identical for all three specimens.

During the deviatoric stress phase, the results of the tests are different due to different confining stresses. It is possible to identify the onset of dilatancy by the evolution of volumetric strains (as shown in the example of Fig. 5). In all three tests, the onset of gas flux is measured at higher deviatoric stress levels than the onset of dilatancy (compare Fig. 5 and 6). The boundary for the failure of the specimen increases with higher confining stress, analogue to the onset of dilatancy (Fig. 7). The onset of gas flux and the failure of the specimens occurred nearly at the same deviatoric stress level.

Consequently, the test results show that the investigated salt concrete samples were gas-tight until the load limit was reached. Generally, no damage is expected in the salt concrete specimens below deviatoric stresses of 30 MPa.

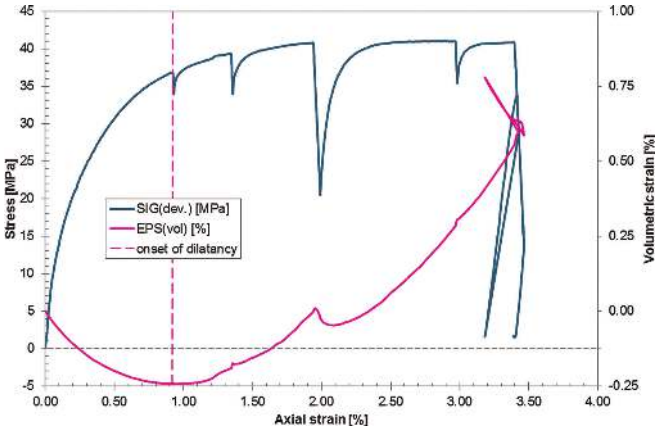

Fig. 5. Stress-strain behaviour of a salt concrete sample deformed by deviatoric loading at confining stress of 3 MPa

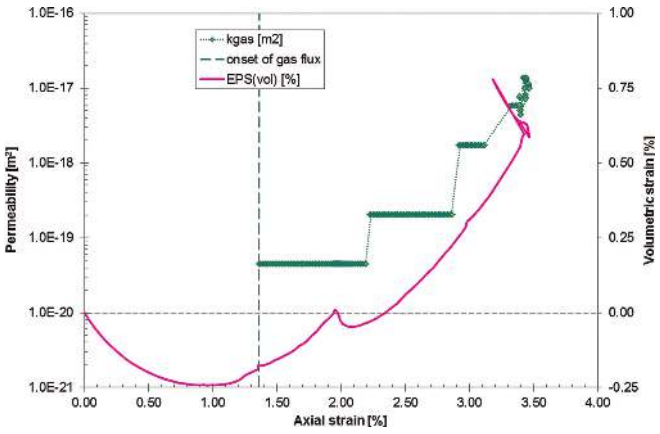

Fig. 6. Strain-permeability behaviour of a salt concrete sample deformed by deviatoric loading at confining stress of 3 MPa

3.2 Long-term deformation behaviour of salt concrete

The tests aim at determining the deformation of the samples in terms of strains and strain rates in order to describe the time-dependent uniaxial creep behaviour of salt concrete at different stress states.

3.2.1 Experimental layout and testing procedure

Uniaxial creep tests were performed in a rig in an air-controlled room. The rig allowed five samples of 80 mm in diameter and 160 mm in length being simultaneously tested at the same load up to 500 kN at ambient temperature. Figure 8 shows the rig for uniaxial creep tests on five samples. Axial load was applied equally to the five samples by means of an oil balance with an accuracy higher than ±0.5 %. Axial deformation of each sample was originally measured by displacement transducers (LVDT) with an accuracy of ±0.1 mm. Radial strains were measured by strain gauges of a resolution of 10^{-6}. They were directly glued on the samples.

In the following analysis, only the results for axial deformation measured by LVDT are considered. The reason for this approach is that the LVDT measure the change of the whole length of the specimen while the strain gauges measure only a fraction. Thus, the measurement with the LVDT is more representative for the overall sample behaviour. The denotations SC(1048) up to SC(1052) serve as identification for the individual specimens of the uniaxial tests.

The tests were executed at three different stress states. First, the axial stress was set to 5 MPa. The following steps were performed at 10 MPa and 20 MPa, respectively. During the tests the temperature was held at approximately 25 °C. The axial stress causes a reduction of the length and an increase in diameter of the specimens.

All tests lasted over nearly 300 days with a duration of 76 to 106 days for each step. Uniaxial strain-time curves measured on 5 samples are illustrated in Fig. 9, whereas the stress and temperature boundary conditions are shown in Fig. 10.

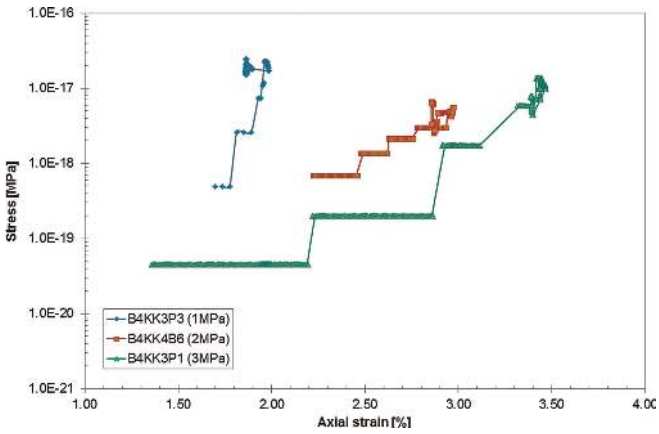

Fig. 7. Strain-permeability curves obtained on the salt concrete samples at different confining stresses

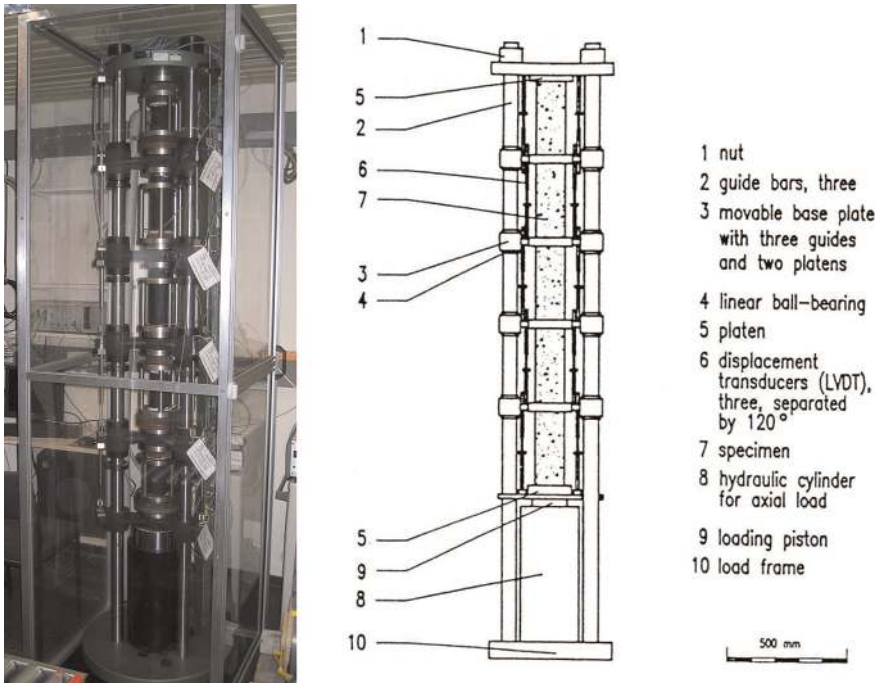

Fig. 8. Rig for uniaxial creep tests on a stack of five samples

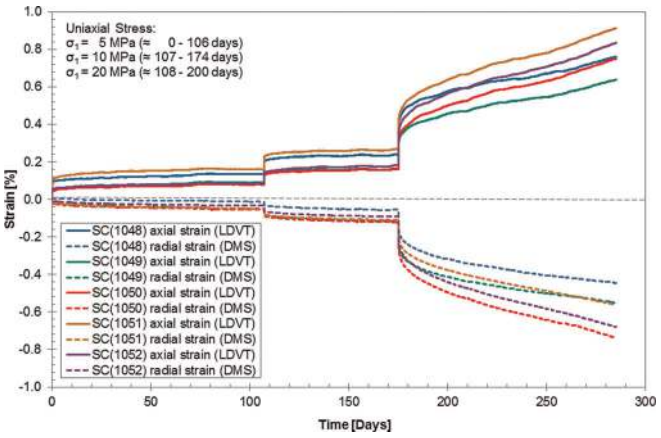

Fig. 9. Long-term uniaxial creep behaviour of five salt concrete samples under multi-step loads – axial and radial strains

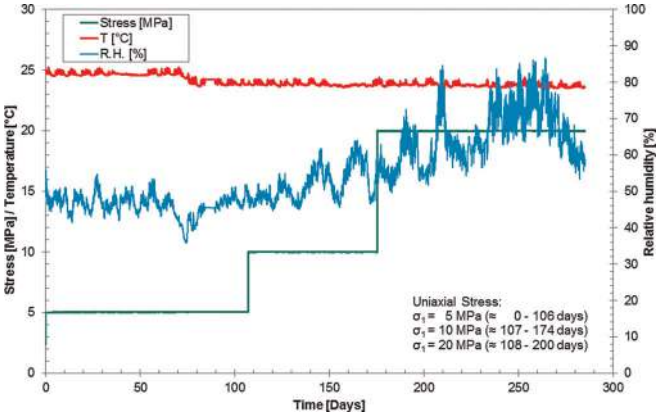

Fig. 10. Long-term uniaxial creep behaviour of five salt concrete samples under multi-step loads – stress, temperature and relative humidity evolution

3.2.2 Measurement results and interpretation

Figure 11 shows the axial strain and the strain rate as a function of time for a representative sample. Strain rate is averaged over seven days. The figure shows that at the first two stress levels strain scarcely increases while strain rates quickly decrease. That means that there is no stationary creep. Strain increases at the third stress level, and strain rate seems to stabilize in the range of $10^{-10}\,s^{-1}$, which could imply a steady state creep at this stress level.

The results of the uniaxial creep test show that material behaviour is different at lower stress levels of 5 MPa and 10 MPa and at a stress level of 20 MPa. While strains are small at lower stresses, a distinct creep deformation occurs at a stress level of 20 MPa.

The reason for the different deformation behaviour at various stress levels might be that the cement structure of the salt concrete bears at uniaxial stresses up to 10 MPa. Cement is expected to have an elastic material behaviour without visco-plastic deformations after the water curing process has finished. Therefore, no stable creep rates could be derived at lower stress.

When the stress level was increased up to 20 MPa, the cement structure of the salt concrete was damaged. Consequently, the salt grit structure of the salt concrete was subjected to the load, and because of the visco-plastic material behaviour of salt grit the specimens exhibited explicit creep behaviour.

3.3 Evolution of combined salt concrete/rock salt system

3.3.1 Experimental layout and testing procedure

For performing experiments on the system consisting of a salt concrete seal element and the surrounding dilated rock salt at the laboratory scale, the idea is to use hollow salt cylinders furnished with a central core of salt concrete which are placed in isostatic cells to impose confining stress. Thus, a combined sample represents the system of seal element, contact seam and surrounding rock at a small scale. The salt concrete core

(35 mm in diameter) is placed in the hollow cylinder (70 mm in outer diameter and 100 mm in height) with a snug fit. In order to fill up potentially remaining voids, the core is coated with salt slurry and then pushed into the hollow salt cylinder. Excess slurry is removed and the sample is dried in an oven to avoid undefined saturation states. A photo of a salt concrete core, a hollow cylinder and the completed sample is shown in Fig. 12.

The samples are coated with rubber jackets and placed in isostatic cells equipped with hydraulic lines to allow for axial flow-through of gas or liquid and determination of the system permeability.

The test procedure is first to perform gas permeability tests of the dry sample while stepwise increasing the compressive load. After unloading the sample saturated brine is injected and the stepwise loading is repeated, while the permeability of the seal system to brine is recorded. The evolution of the permeability of the composite sample to gas or to brine is the essential variable characterizing the recovery of the EDZ and the closing of the contact seam between salt concrete core and surrounding rock salt.

A pilot test was performed in order to check whether the sample composition and the measurement technique were suitable. After the test, the sample was dismantled and inspected. The pilot test showed that the test method is adequate to investigate evolution of the overall permeability of dry and brine-containing composite samples as a function of compressive load. It also showed that load changes have to be applied cautiously in order to maintain integrity of the testing arrangement.

For the start of detailed testing, two new samples were prepared. In order to increase the bandwidth of results, one sample featured an intact salt concrete core as taken from the in-situ seal, while for the other sample a larger salt concrete core was loaded triaxially to the failure point and a smaller core was machined from the damaged core. The rationale of using a damaged salt concrete core as seal element is the fact that shrinkage fractures of a seal during construction cannot be excluded.

Both the salt concrete cores and the rock salt cylinders were characterized in terms of permeability to gas before preparing the combined samples. Afterwards, gas and liquid testing in the isostatic cells was started similarly to the pilot test.

For characterization of the salt concrete cores, these were placed in isostatic cells and the load dependent gas permeability was determined under stepwise loading from 1 to

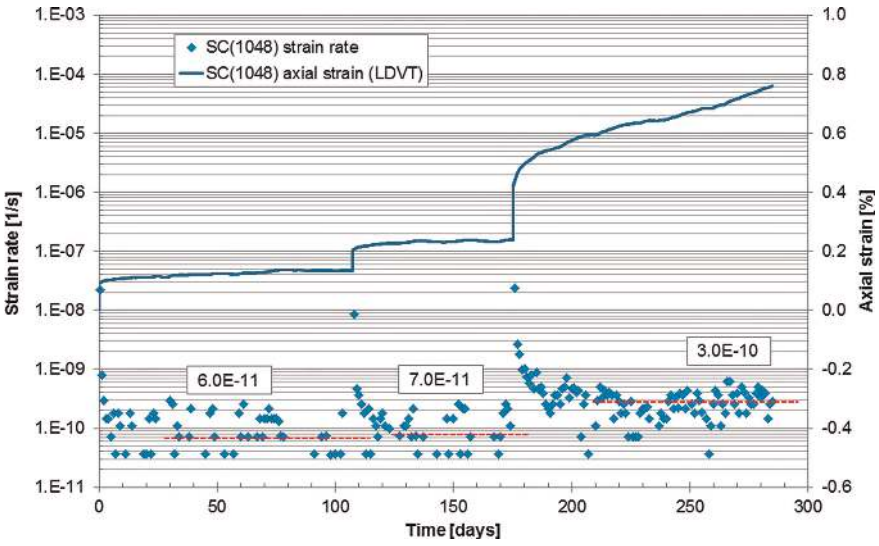

Fig. 11. Long-term uniaxial creep behaviour of salt concrete sample no.1048 under multi-step loads – axial strain and derived creep rates

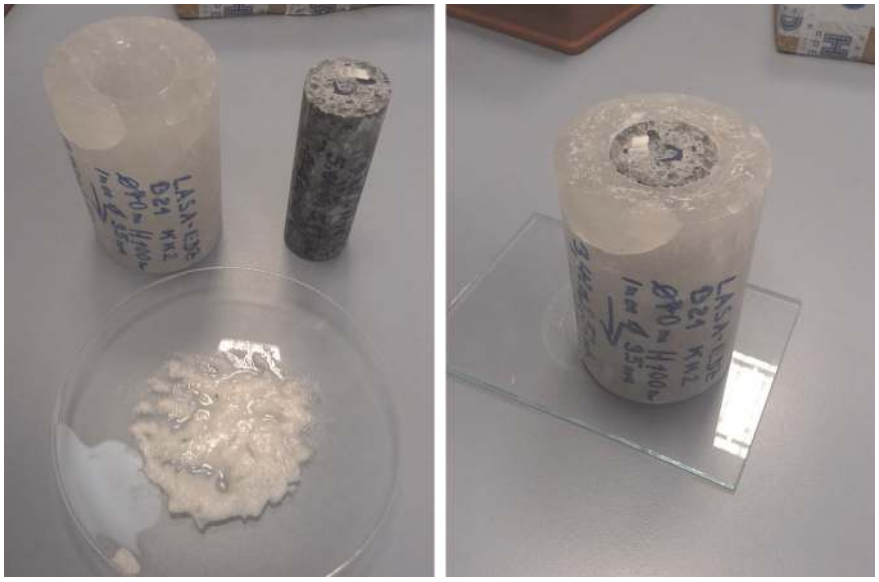

Fig. 12. Hollow salt cylinder, salt concrete core and salt slurry (left); complete combined sample (right)

5 MPa. The permeability of the intact salt concrete core, calculated using Darcy's law, amounted to $2.3 \cdot 10^{-20}\,m^2$ at 1 MPa isostatic load and fell below $10^{-22}\,m^2$ already at 2 MPa. This also showed that flow along the jacket interface is not an issue. For the damaged core, a moderate permeability decrease from $4.1 \cdot 10^{-18}\,m^2$ at 1 MPa load to $1.6 \cdot 10^{-18}\,m^2$ at 5 MPa was observed.

The salt cylinders were subjected to the same tests before drilling the central holes for reception of the salt concrete cores. They also showed a permeability decrease with load: From $2.6 \cdot 10^{-19}\,m^2$ to $2.5 \cdot 10^{-21}\,m^2$ for the cylinder used with the intact salt concrete core and from $5.2 \cdot 10^{-20}\,m^2$ to below $10^{-22}\,m^2$ for the cylinder used with the damaged one.

The results of the load-dependent permeability tests of the individual material samples are summarized in Fig. 13.

After characterization of the salt concrete and salt cores, the central holes were drilled into the salt cylinders and the combined samples were prepared as described earlier (see Fig. 12). The potential effect of the sub-coring on the salt core gas permeability could not be quantified.

3.3.2 Measurement results and interpretation

In the first stage of testing the combined samples, the confining load was increased by 1 MPa steps to 5 MPa over two weeks and gas flowed axially through the samples. For the sample with the intact seal element of salt concrete, the gas permeability decreased slightly from $2.5 \cdot 10^{-14}\,m^2$ to $1.3 \cdot 10^{-14}\,m^2$. When the sample was unloaded, the gas permeability remained at this value. The permeability measured was close to the upper limit of the testing arrangement. In fact, for the sample with damaged seal element gas permeability remained above the upper measurement limit of $5 \cdot 10^{-14}\,m^2$.

The gas tests on dry samples showed the high impact of the contact seam – the overall permeability was much higher than the gas permeabilities of the individual materials. A second result of gas testing was that under dry conditions and moderate confining stress up to 5 MPa, a reconsolidation of the EDZ or a closing of the contact seam is negligible in the short term.

After gas testing, the samples were unloaded and brine was injected. Then, the samples were again loaded in steps of 1 MPa up to 5 MPa, and the permeability to brine was measured. The measurement results are shown in Fig. 14. The time until maximum load was three weeks for the two samples. Both samples showed a significant decrease of permeability to liquid with increased loading.

For the sample with the intact seal element, permeability decreased from an initial value of $4.5 \cdot 10^{-15}\,m^2$ to below the detection limit of $10^{-20}\,m^2$ at a load of 5 MPa. Obviously, the salt surrounding the seal element became soft enough to enable very effective sealing of the contact seal and the EDZ in short time. The sample behaved significantly different from the dry case, where only a slight gas permeability reduction was observed.

Afterwards the sample was stepwise unloaded again. Permeability remained below the detection limit, showing that irreversible compaction had occurred. It is envisaged to dismantle the sample and confirm the reconsolidation and associated reduction of pathways by microscopic inspection.

As expected, the sample with the damaged seal element started at a higher permeability of $3.6 \cdot 10^{-13}\,m^2$ (please note that the measurement limits for permeability measurement with liquid are different from those for gas tests). With increasing confining stress the permeability decreased by two orders of magnitude, but it remained much higher than for the sample with the intact seal element.

While a compressive load of 5 MPa was sufficient to effectively seal the contact zone and the EDZ in the presence of brine in the experiment with the intact seal element, the same cannot be postulated for the experiment with the damaged seal element. Obviously, reconsolidation of the damaged seal element has not been achieved. The permeability value measured at 5 MPa confining stress, however, seems too high to attribute it to the flow through the seal element alone, as the gas permeability of the damaged salt concrete ranged between $10^{-18}\,m^2$ and $10^{-17}\,m^2$ (see Fig. 13).

This sample was not unloaded. The confining stress was increased in steps up to 10 MPa and the measurement of permeability to brine continues. Figure 15 shows the permeability to brine as a function of time. Obviously, the permeability value decreased not only with increasing confining pressure (light grey phase). The measurements showed a decrease of more than 2 orders of magnitude from $10^{-15}\,m^2$ down to $10^{-18}\,m^2$

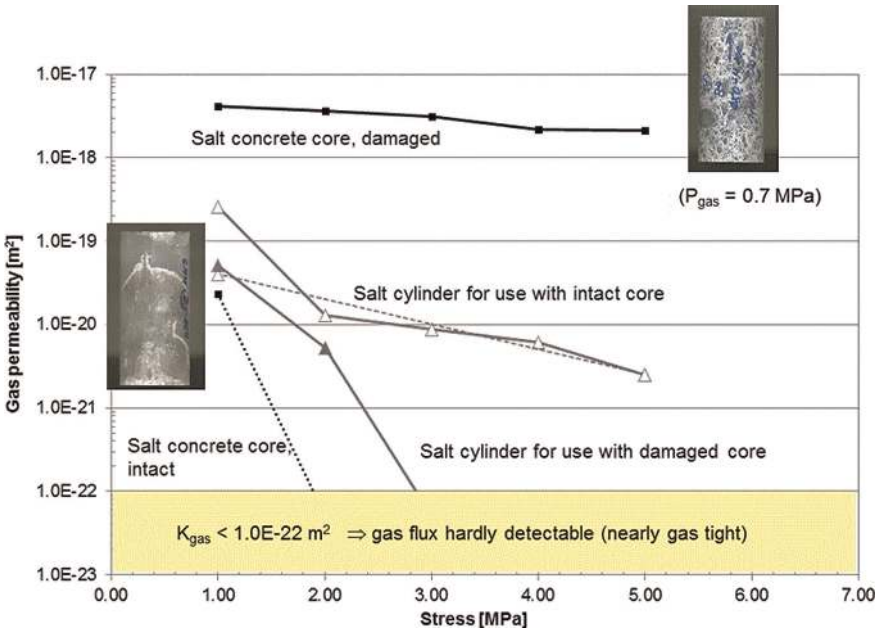

Fig. 13. Gas permeability of salt concrete cores and salt cylinders before assembly of combined samples

within the next 100 days (2400 hours). It is expected, that the permeability value will tend towards the detection limit without further increase of the confining pressure. Extensive calculation activities are underway for interpretation and further prognosis of the experimental data.

3.4 Long-term chemical stability

The chemical stability of cement-based sealing materials is of vital importance for the longevity of sealing elements. In case of an enduring contact between aqueous solution and the sealing element, dissolution and precipitation processes can occur which eventually might result in changes of porosity and subsequently mechanical stability. Two evolutions are conceivable: firstly, the porosity and consequently the permeability could increase. This may lead to a loss of mechanical stability. Secondly, the porosity could decrease due to a net increase of solid phase volume. This would result in a decrease of permeability [6].

The composition of solution depends on the ambient host rock formation. For the present considerations the most important mineral phases in salt rock are halite (NaCl), anhydrite ($CaSO_4$), gypsum ($CaSO_4 \cdot 2H_2O$), sylvite (KCl), kieserite ($MgSO_4 \cdot H_2O$), polyhalite ($K_2Ca_2Mg\ [SO_4]_4 \cdot 2H_2O$), carnallite ($KMgCl_3 \cdot 6H_2O$) and kainite ($K_4Mg_4[Cl_4SO_4]_4 \cdot 11H_2O$). Naturally occurring brines in equilibrium with rock salt are always saturated with respect to halite. Equilibration with other mineral phases lead to quinary solutions (without Ca) or hexary solutions (with Ca) with compositions specific for the particular set of mineral phases the solutions has equilibrated with. In contact with potash salts the formed brines are dominated by Mg^{2+} and Cl^- [7].

The corrosion mechanism of sealing elements depends significantly on the used construction material and on the solution composition. NaCl-based salt concrete is stable against solutions, which are in equilibrium with halite only, or in equilibrium with halite and $CaSO_4$-phases (hereafter referred to as "NaCl-solution"), but corrodes in the presence of high $MgCl_2$-concentrations. A specific $MgCl_2$-rich solution in equilibrium with halite, sylvite, carnallite, kainite, and polyhalite is of particular interest and hereafter referred to as "Mg-rich-solution". $MgCl_2$-based sorel cement shows an opposite behav-

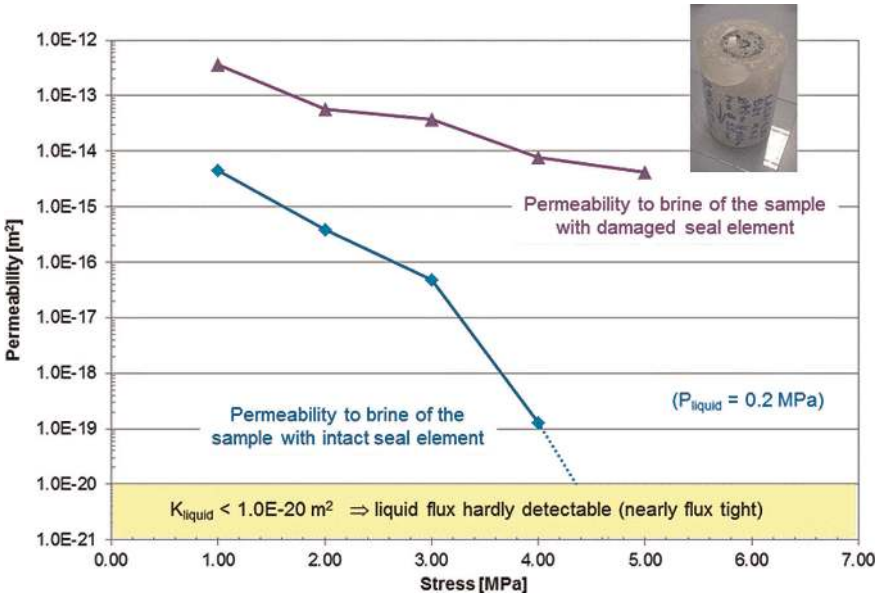

Fig. 14. Permeability of combined samples as a function of confining stress

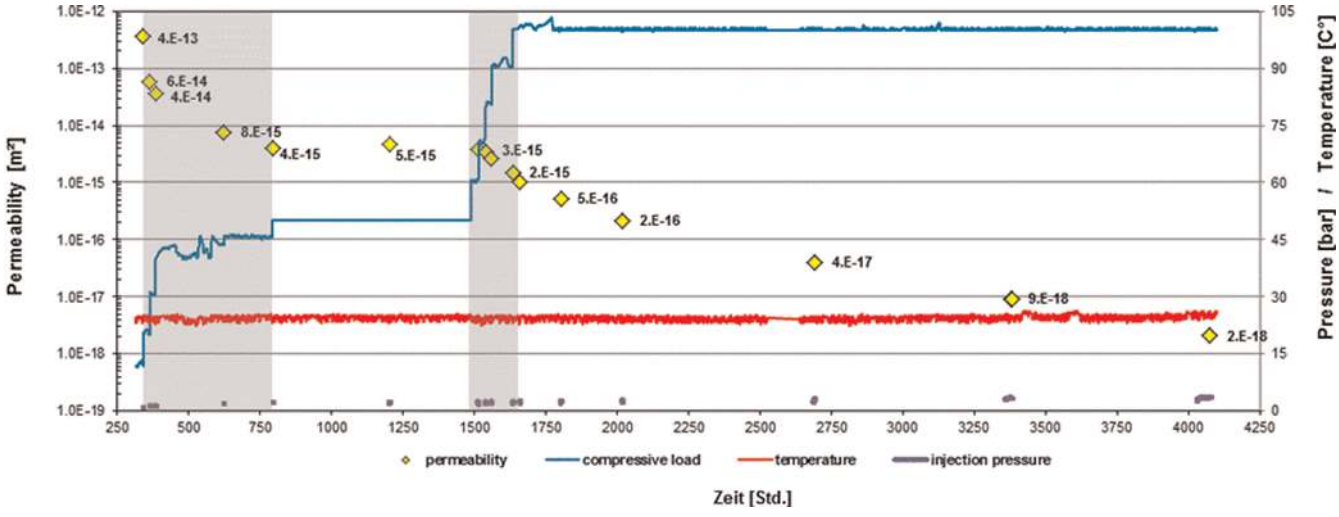

Fig. 15. Permeability to brine of the sample with damaged seal element as a function of time

iour to salt concrete: it tends towards to be stable in Mg-rich-solution and corrodes in NaCl-solution containing [8].

Laboratory tests executed by GRS aim at investigating the reaction path and the diffusive and advective transport mechanism in salt and sorel concrete in contact with Mg-rich- and NaCl-solutions. The experiments described in the following are currently performed in the GRS laboratory.

3.4.1 Geochemical experiments

Experimental layout

"Cascade experiments" are executed to investigate the reaction path between sealing material and solution. The cascade experiment is a sequence of batch-experiments and has to be performed in air-tide vessels for the elimination of carbon dioxide.

In any batch-experiment powdered concrete is exposed to solution in a defined solid-solution-ratio. Vessels are shaken in an over-head-shaker during the whole reaction time. If equilibrium is reached between concrete and solution, the solution is separated from solid and is exposed to new powdered concrete for the next cascade and in the same solid-solution-ratio as before. This process is repeated until no free aqueous solution can be regained anymore after an equilibration step. Solution and solid phases are analysed at the end of each cascade. The test procedure is schematically illustrated in Fig. 16.

The total chemical reaction path of solution penetrating a geotechnical barrier can be reproduced by the cascade experiment until thermodynamic equilibrium between the original solution and the solid material is attained. In this way, chemical reactions which may occur by an intrusion of brine to a sealing element can be simulated in very short time [9].

Singular batch-experiments have been executed before starting the cascade experiments. This aimed at determining the reaction time between solution and concrete until the equilibrium is reached. Therefore, four preparations (in PE-bottles) in each system (sorel concrete/Mg-rich-solution, sorel concrete/NaCl, salt concrete/Mg-rich-solution, salt concrete/NaCl) were prepared. The bottles were shaken by hand every day. Samples were taken after 2, 4, 7, 9, 11 and 18 days.

Preliminary measurement results and interpretation

Figure 17 shows the x-ray-diffraction (XRD) diagrams of sorel concrete before contact with NaCl-solution and Fig. 18 shows results after 11 days. The comparison of these diagrams shows clearly the dissolution of sorel concrete typical 3-1-8-phases ($3Mg(OH)_2 \cdot MgCl_2 \cdot 8H_2O$) and the development of new phases. These new phases are currently unknown. Further change in phase composition has not been observed after 11 days. The analysis of the solution has revealed no significant change in its composition over total testing time. Consequently, each cascade in the cascade experiment in system sorel concrete/NaCl-solution needs at least 11 days. Equilibration time between sorel concrete and NaCl-solution is only valid for a system with powdered concrete, for solid samples a longer equilibration time is expected because of the significant smaller specific surface.

Contrary to expectations the investigation of system sorel concrete/Mg-rich-solution shows a change in solution composition. Concentrations of Na, Cl, Mg, K and SO_4^{2-} have decreased during the test. Figure 19 shows exemplary the development of Cl- and Mg-concentrations.

Figure 20 shows the results of the experiments in the system salt concrete/Mg-rich-solution. A clear increase of Ca-concentration can be identified resulting from the dissolution of salt concrete typical CSH-phases in consequence of a Mg-attack. Additional K-concentration has also increased during concentration of Mg and Cl has decreased (chemical processes are explained in section 3.4.2).

As expected the investigation of the system salt concrete/NaCl-solution shows no significant change in solution and phase composition.

3.4.2 Hydraulic experiments – Through-diffusion-experiments

Experimental layout

Through-diffusion-experiments are executed in special diffusion cells. A simplified schematic depiction is shown in Fig. 21. The concrete sample is installed in the diffusion cell and a tracer-spiked brine is passed on the bottom of the sample. A second, non-spiked brine is passed on the top of the sample and is analysed with regard to its development of tracer concentration over time. Because of the concentration difference between brine 1 (spiked) and brine 2 (non-spiked) a diffusional transport of tracer molecules from the bottom to the top of the sample is expected.

The diffusion coefficient can be calculated on the basis of these experimental data. The thickness of samples and the

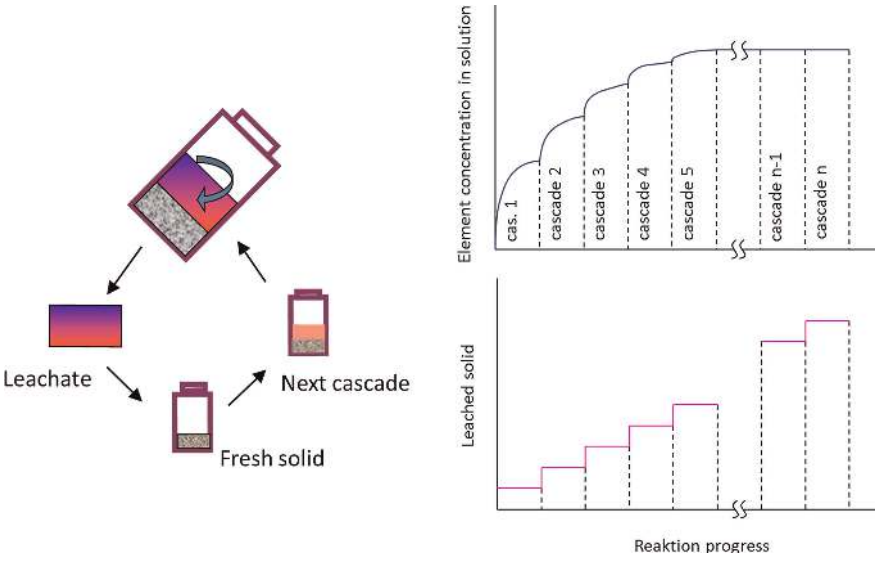

Fig. 16. Test procedure of the GRS cascade experiment [12]

duration necessary for saturation prior to starting diffusion experiments is determined in preparatory experiments.

Through-diffusion-experiments aim furthermore at investigating the kinetics of chemical reactions by diffusive corrosion processes. In principle, two scenarios are conceivable: on one hand a parallel progression of diffusion and corrosion may occur, on the other hand diffusion may occur faster than the process of corrosion. This circumstance will be investigated by analyses of the solid sample using x-ray diffraction. Through-diffusion-experiments are in progress.

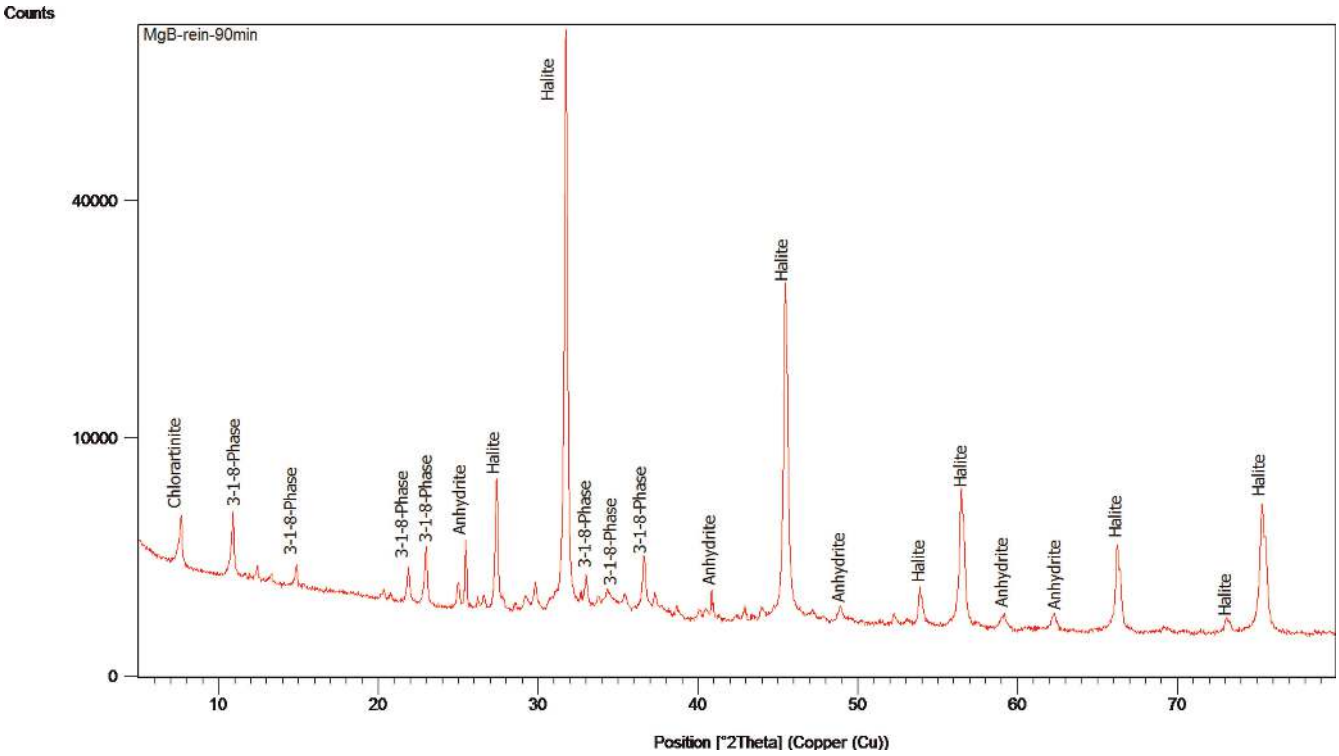

Fig. 17. XRD-diagram of sorel concrete A1 before contact with solution

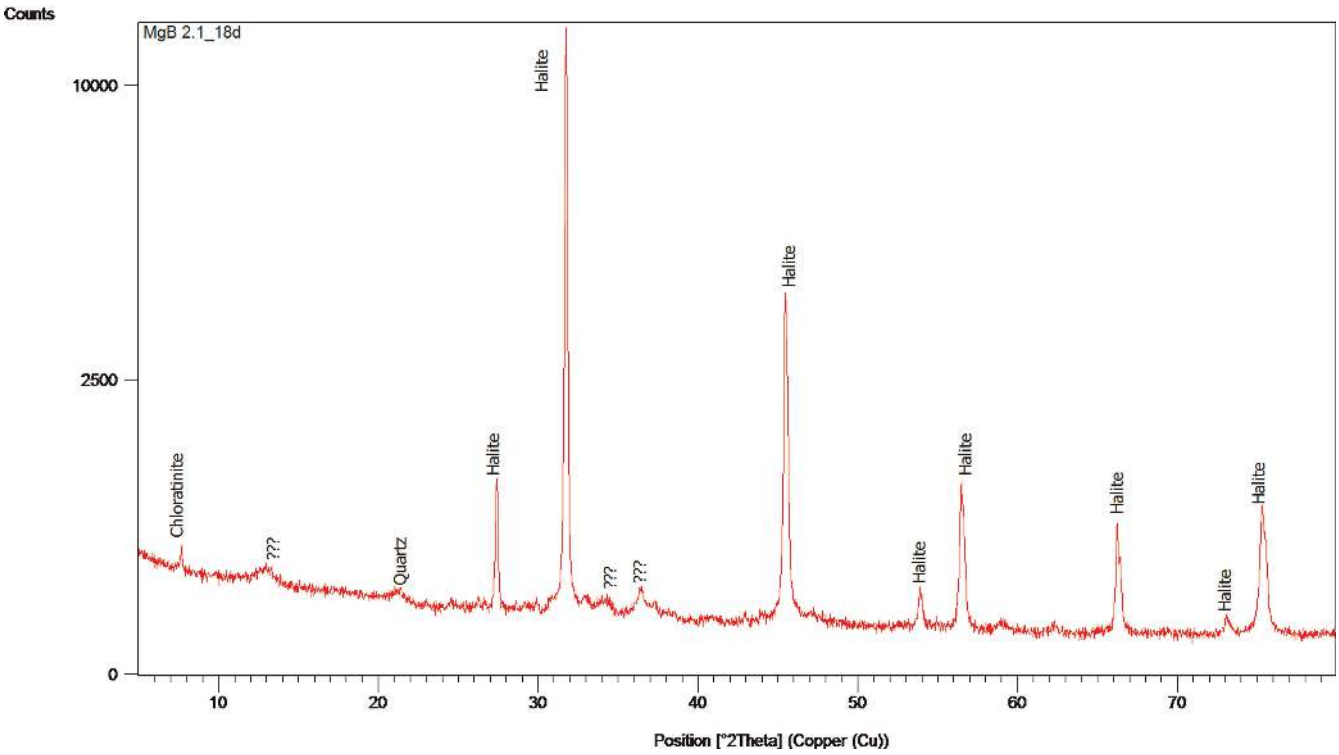

Fig. 18. XRD-diagram of sorel concrete A1 after contact with NaCl-solution

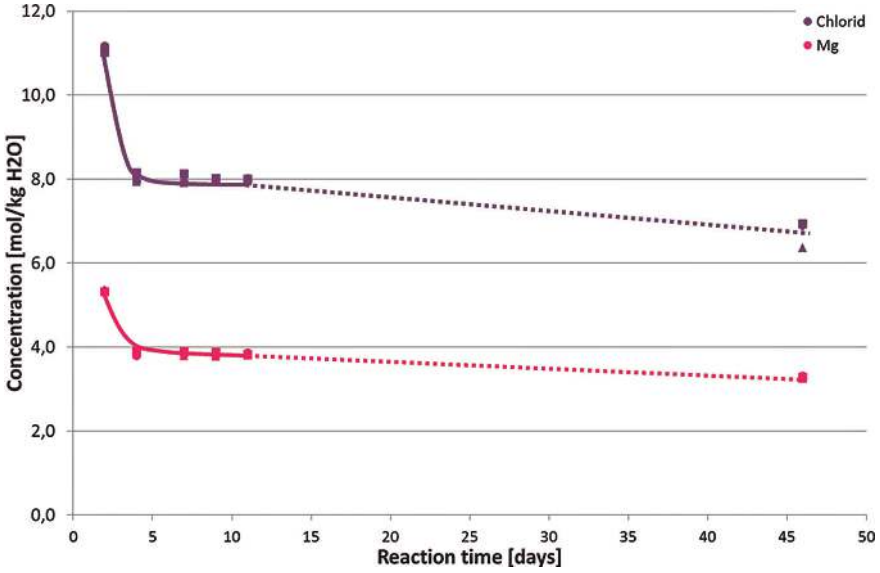

Fig. 19. Development of Cl- and Mg-concentrations of solution in the system sorel concrete/Mg-rich-solution

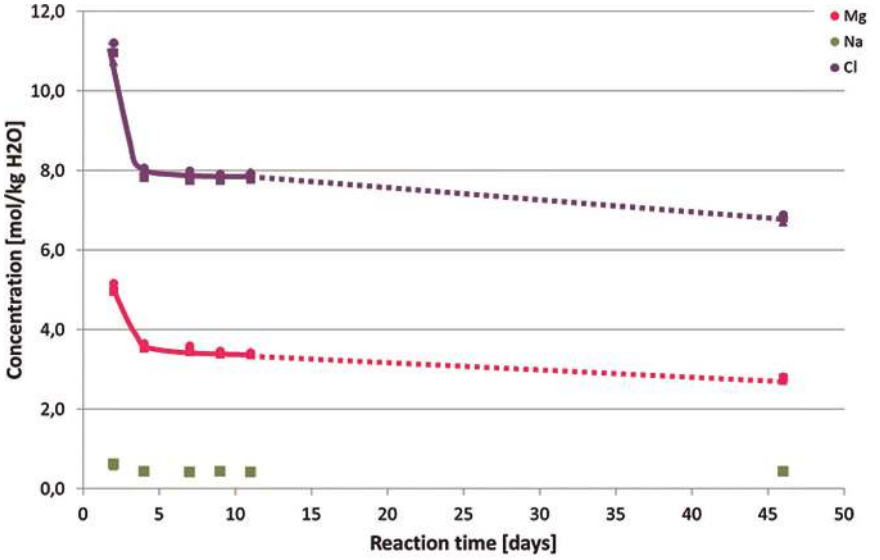

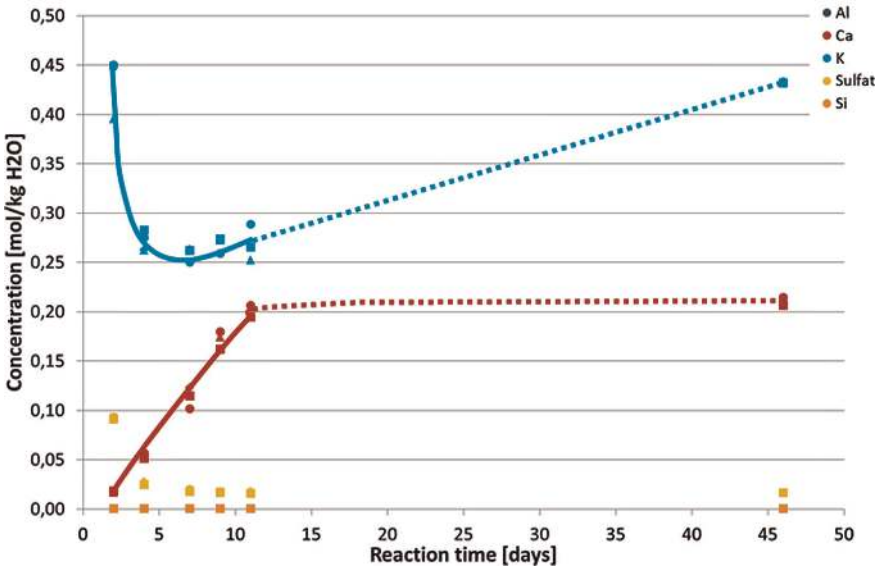

Fig. 20. Development of solution composition in the system salt concrete/Mg-rich-solution

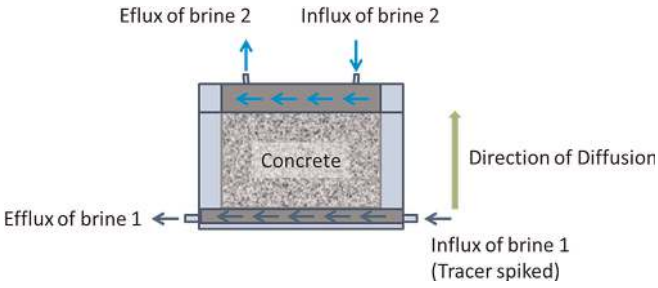

Fig. 21. Simplified construction of a diffusion-cell

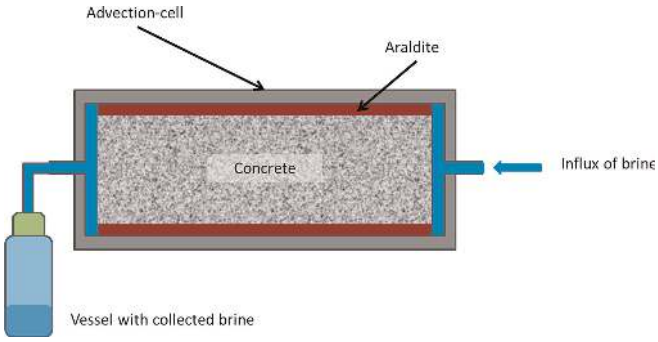

Fig. 22. Simplified construction of an advection cell

3.4.3 Hydraulic experiments – Advective corrosion experiments

Experimental layout

Advective transport is another transport mechanism in porous media which may affect corrosion of sealing elements. Corrosion as a result of advective transport and its consequences for the long-term sealing capacity will be investigated in two types of advection experiments: experiments which aim at reaction kinetics similar to diffusion experiments and experiments for investigating the influence of corrosion on porosity and permeability of the sealing material.

A concrete sample with 100 mm in length and 50 mm in diameter is loaded with fluid pressure (NaCl-/Mg-rich-solution) on one end face in the first type of advection experiments. The effluent brine is collected on the other face. The sample surface is pressure-less cast in araldite in an advection cell. A simplified sketch of an advection cell is shown in Fig. 22.

In regular intervals permeability is measured and vessels for collecting brine are substituted. The individual brine samples will be analysed with regard to their composition. Additionally, the composition of each concrete sample will be investigated by decomposition and x-ray-diffraction. A conclusion and better understanding of corrosion mechanisms affected by advection processes in concrete is expected from these experiments.

The installation of the second advection experiment is very similar to the first experiment. The main difference is that the cylindrical concrete samples are surrounded by rock salt, thus exhibiting a circular contact zone. It is assumed that the contact zone is the primary pathway for brine and for the migration of nuclides. Samples are 100 mm in length and 70 mm in diameter with a concrete core of 35 mm in diameter.

For these tests samples of the hollow rock salt cylinders with a salt concrete core described in section 3.3 are used (see Fig. 12). Samples are exposed to a confining pressure until permeability is minimized. This process simulates salt creep on the sealing element. Afterwards, samples are placed in advection cells in the same manner as described before for concrete samples.

A further experiment on combined samples (salt concrete/rock salt) is in progress (Fig. 23). In phase 1 a confining pressure of 5 MPa in the beginning and of 10 MPa in further process was brought to the sample. During compaction the sample has been in contact to a NaCl-solution. After the contact zones were closed up to a permeability of 10^{-18} m^2/s, radial pressure was minimized to 2 MPa for minimizing the creep effects. In the next step (phase 2 and 3), NaCl-solution was changed to a Mg-rich-solution and development of permeability was occupied.

Preliminary measurement results and interpretation

Current results from advection experiment with sorel concrete and NaCl- and Mg-rich-solution are available and de-

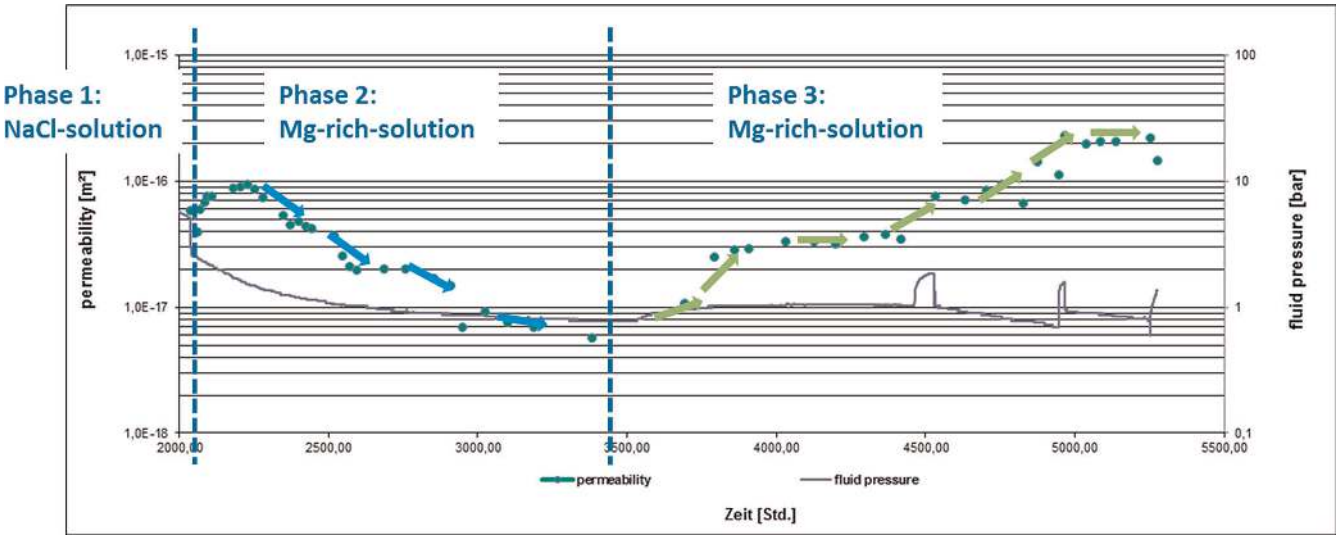

Fig. 23. Development of permeability of a combined sample (salt concrete/rock salt). Phase 1:. Flow of NaCl-brine and compaction of sample. Phase 2: Change to Mg-rich-solution and decrease of permeability. Phase 3: Increase of permeability

picted in Fig. 24 and Fig. 25. They show the development of permeability to NaCl- respectively Mg-rich-solution flowing through. Gas permeability has been in the same order (around $1 \cdot 10^{-18}$ m^2) for all samples when experiments were started so that a similar permeability to solution was expected for each sample. Sorel concrete in contact with NaCl-solution was very quickly permeable to solution. Permeability has been measurable in all samples after seven to sixty days and permeability increased constantly in all samples (compare Fig. 23). A permeability of $1 \cdot 10^{-17}$ m^2 was reached in samples AS 31-1, AS 34-2 and AS 36-1 after a solution volume of about 250 ml has passed the samples. It increased by a magnitude of a half to one. Permeability of samples AS 32-5 and AS 34-1 was less – at around $5 \cdot 10^{-18}$ m^2 – after a flow through of 250 ml solution. Core AS 31-2 had the lowest initial permeability but the highest permeability increase proportional to volume of passed through solution. Permeability increased over one magnitude. Permeability increased to $1 \cdot 10^{-18}$ m^2 after 60 ml of NaCl-solution had passed the sample. Afterwards, permeability increased slower. Figure 24 shows the development of permeability of sorel concrete in contact with Mg-rich-solution. This experiment was executed in parallel to the experiment with NaCl-solution so that samples were exposed at the same time to potential attack by solution. Permeability was at $1\text{-}5 \cdot 10^{-19}$ m^2 in AS 31-8 and AS 34-1 and was measurable after 200 to 250 days. In sample AS 36-2 permeability was constantly at $5 \cdot 10^{-19}$ m^2 over 250 days. Then permeability increased suddenly up to $8 \cdot 10^{-17}$ m^2 after circa 170 ml of passed through solution. It decreased in the meantime to initial permeability again and increased afterwards clearly over one and a half magnitude. Three further samples have been tested. After circa 365 days a flowing through could be detected. But mass of collected brine is too small for the calculation of permeability until now.

Results from advection experiments confirm that sorel concrete is not stable against NaCl-solutions which is known from former investigations. Corrosion occurs by the dissolution of 3-1-8 phases, which results in an increase of porosity and consequently permeability. X-ray diffraction of the sorel concrete from batch-experiments have shown this process of sorel phase dissolution well (compare Fig. 17 and Fig. 18). In a next step unknown phases need to be identified.

Investigations of sorel concrete in contact with Mg-rich-solution show a much better resistance. But according to former batch-experiments the corrosion of sorel concrete could not be excluded completely because of the development of per-

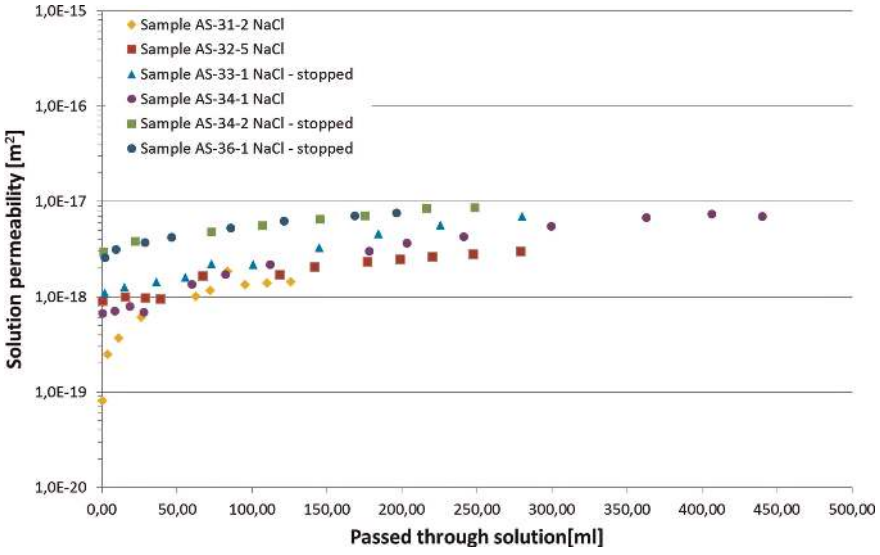

Fig. 24. Development of permeability of sorel concrete to NaCl-solution

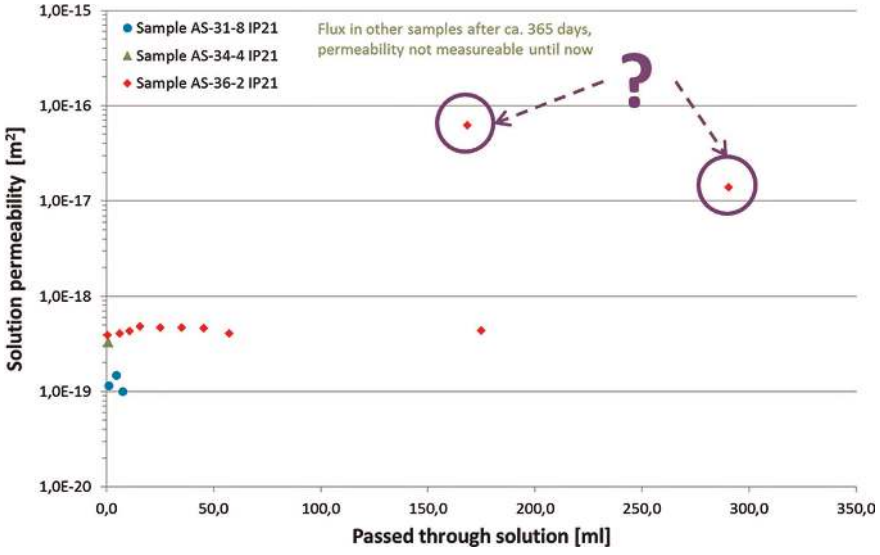

Fig. 25. Development of permeability of sorel concrete to Mg-rich-solution

meability. One hypothesis is that the flux in advection experiments results of connected pore spaces so that Mg-rich-solution flows very slowly through the samples under injection on pressure without corrosion. Constant permeability in AS 31-8 and AS 34-1 argues for it. It should also be considered that very slow corrosion processes may occur because of the permeability increase in AS 36-2. This hypothesis is supported by results from batch-experiments. Hence, the analyses of the development of solution composition and x-ray-diffraction have to be awaited.

Figure 23 shows measuring results from advection experiment on combined sample salt concrete/rock salt. At the beginning of the experiment permeability of the combined sample has been reduced by a surrounding pressure and flow through of NaCl-solution (phase 1). After solution has been changed to a Mg-rich-solution, permeability suddenly increases by two orders of magnitude and decreases by one order of magnitude when injection pressure was reduced. After two month of contact with Mg-rich-solution the permeability starts to increase again. This phenomenon results from chemical processes in salt concrete as former investigations at GRS have shown. It is assumed that the high injection pressure in beginning of phase 2 has generated the increase of permeability. May be chemical processes could not proceed because solution has passed the sample faster than processes need for their reaction. After injection pressure has been reduced, chemical processes could proceed. If the Mg-rich-solution is brought in contact with salt concrete, free hydroxide (OH^-) is fixed by magnesium and brucite ($Mg(OH)_2$ is precipitated. Now pores are clogged by brucite and the pH decreases to 8–9 (phase 2). As a result of the pH decrease portlandite ($CaOH)_2$ becomes instable and decomposes in Ca- and hydroxide ions. After consumption of all portlandite the pH decreases further and stabilizing CSH-phases are dissolved. Now concrete loses its stability and permeability starts to increase (phase 3) [9]. Hence, the dissolution of CSH-phases can also be observed in this experiment composition. But dissolution needs more time compared to the batch- and cascade-experiments with powdered concrete.

4 Summary and outlook

The deformation behaviour of salt concrete was investigated by laboratory testing. Therefore, two types of tests were carried out: Triaxial compression tests and uniaxial creep tests. In addition to the laboratory investigations, the tests should be simulated using CODE_BRIGHT and then the calculation results should be compared to the laboratory results. The simulation of the triaxial tests should aim at the investigation of the material changes between the second and third stress level in the uniaxial tests. The comparison of experimental and simulation results should be useful when the onset of dilatancy could be pinpointed.

GRS is investigating the sealing capacity of combined systems of salt concrete seal elements and surrounding rock salt at the laboratory scale. Currently, the following results have been obtained:

- At dry conditions and a moderate confining stress up to 5 MPa, reconsolidation is slow. A potentially existing highly permeable contact seam between the seal element and the rock will not be closed, at least not in the short term.
- With an intact seal element, a confining stress of 5 MPa is, however, sufficient to prevent brine flow along the seal. In the presence of brine, contact seam and EDZ are quickly closed, resulting in overall permeability below 10^{-20} m^2.
- A pre-damaged seal element (e. g. damaged by shrinkage fracturing during construction) will not be re-consolidated at a confining stress of 5 MPa, even if brine is present.
- At a confining stress of 10 MPa and a testing time of 6 month the contact seam and the EDZ are closed with time, resulting in overall permeability below 10^{18} m^2.

The next steps in the experimental investigations will be to dismantle the reconsolidated sample with the intact seal element and to use microscopic methods to investigate pathway reduction. Second, GRS wants to find out at which stress level reconsolidation of the pre-damaged seal element is effective. Finally further experiments have to be performed to investigate variability of results and to derive generally valid material behaviour.

For a numerical simulation of the seal/rock salt system, available physical models of rock salt and salt concrete will be applied to the experiments described here and simulation/improvement cycles will be performed to advance model validation and calibration.

Chemical-hydraulic behaviour of salt and sorel concrete was investigated by various short- and long-term experiments on solid and powdered concrete. Previous investigations show following results:

- Sorel concrete in contact with NaCl-solution develops an increase of permeability and loses its stability because of dissolution of characteristic sorel phases. Secondary phases, which develop, still need to be identified.
- Batch and advection experiments have showen that sorel concrete in contact with Mg-rich solution is not inevitably stable. Conclusion of advection experiments have to be awaited for investigations of solid and fluid samples. By this a better understanding of preliminary experiment results is expected.
- As expected salt concrete in contact with NaCl-solution is stable.
- A Mg-rich-solution leads to a temporary plugging of pores in salt concrete and by this to a retardation of corrosion processes. As intrusion of Mg-rich-solution proceeds CSH phases are dissolved which results in an increase of permeability and a loss of stability of salt concrete.

Following experiments and analyses are planned for a better understanding of the reaction path between concrete and corrosive solution (cascade experiments). Additionally chemical-hydraulic processes at the contact zone between concrete and rock salt by diffusion will be investigated. Advection experiments are planned, too. Secondary phases in sorel concrete after contact to a corrosive solution shall be determined. And finally a comprehensive modelling program is carried out for a better understanding of chemical processes.

Acknowledgements

The authors gratefully acknowledge the funding of the European Commission under FP7 framework programme, contract no. FP7-323273, and the funding received by the Federal Ministry for Economic Affairs and Energy (BMWi), represented by the Project Management Agency Karlsruhe (PTKA-WTE), contract no. 02E11243 and no. 02E11122.

(Received on 23 February 2016)

References

1 *BMU*: Sicherheitsanforderungen an die Endlagerung wärmeentwickelnder radioaktiver Abfälle. Stand 30. September 2010, Bundesministerium für Umwelt, Naturschutz und Reaktorsicherheit (2010)
2 *DOPAS*: DOPAS – full-scale demonstration of plugs and seals, Annex 1: Description of work. Grant agreement no: 323273, Seventh framework programme (2012)
3 *Kudla, W.; Schreiter, F.; Gruner, M.; Jobmann, M.; Bollingerfehr, W.; Müller-Hoeppe, N.; Herold, Ph.; Freyer, D.; Wilsnack, T.; Grafe, F.*: Schachtverschlüsse für Endlager hochradioaktiver Abfälle. ELSA Teil 1 (2013)
4 *Rübel, A.; Buhmann, D.; Kindlein, J.*: Status report on conceptual and integrated modelling activities. DOPAS Deliverable n° 5.6, Contract Number: FP7 – 323273 (2014)
5 *Müller-Hoeppe, N.; Breustedt, M.; Wolf, J.; Czaikowski, O.; Wieczorek, K.*: Integrität geotechnischer Barrieren – Teil 2: Vertiefte Nachweisführung, Bericht zum Arbeitspaket 9.2. Vorläufige Sicherheitsanalyse für den Standort Gorleben, GRS-288, Gesellschaft für Anlagen- und Reaktorsicherheit (GRS) mbH (2012)
6 *Meyer, T.; Herbert, H.-J.; Schmidt-Döhl, F.*: Endlager Morsleben – Korrosion von Salzbeton durch salinare Lösungen. BfS P 180 (2003)
7 *Herbert, H.-J.*: Zur Geochemie und geochemischen Modellierung hochsalinarer Lösungen mineralischer Rohstoffe. Geologisches Jahrbuch Reihe D, Heft SD 1, ISBN 3-510-95845-4 (2000)
8 *Krauke, W.; Fliß, T.*: Stilllegung ERAM – Konzeptplanung und Nachweisführung für ein Abdichtungsbauwerk im Hauptanhydrit aus Magnesiabinder. BfS (2008)
9 *Niemeyer, M.; Wilhelm, S.; Hagemann, S.; Herbert, H.-J.*: Stilllegung ERAM – Zusammenfassende Auswertung von Experimenten und Modellrechnungen zur Korrosion von Salzbeton mit IP21-Lösung. BfS (2014)
10 *Stahlmann, J.; Mauke, R.; Mohlfeld, M.; Missal, C.*: Monitoring of Sealing Dams – Experiences from a Test Set-Up at the Repository ERAM, Germany: Monitoring in Geological Disposal of Radioactive Waste: "Objectives, Strategies, Technologies and Public Involvement". International Conference and Workshop, March 19 – 21, 2013, Luxembourg
11 *Müller-Hoeppe, N.*: Untersuchungen der Kontaktzone am ASSE-Vordamm – Gesamtinterpretation. Deutsche Gesellschaft zum Bau und Betrieb von Endlagern (DBE) (2010)
12 *Meyer, T.; Herbert, H.-J.*: Full scale demonstration of plugs and seals (DOPAS), Deliverable D3.29 and D5.5. (2014)

The authors of this contribution

Kyra Jantschik (corresponding author),
Dr. Helge C. Moog, Dr. Oliver Czaikowski, Klaus Wieczorek
E-mail: kyra.jantschik@grs.de
Gesellschaft für Anlagen- und Reaktorsicherheit (GRS) gGmbH
Theodor-Heuß-Straße 4
38122 Braunschweig
Germany

Bibliography
DOI 10.3139/124.110721
KERNTECHNIK
81 (2016) 5; page 571 – 585
© Carl Hanser Verlag GmbH & Co. KG
ISSN 0932-3902

Books · Bücher

Performing Safety Culture Self-Assessments. IAEA Safety Reports Series No. 83, Published by the International Atomic Energy Agency, 2016, ISBN 978-92-0-101515-0, 157 pp., 63.00 EUR.

The objective of this Safety Report is to provide practical guidance, building on good practices worldwide, on how to use Safety Culture Self-Assessments (SCSAs) to enhance organizational learning and safety performance. It draws on experience from behavioural, social, psychological and organizational sciences to emphasize the importance of describing aspects of an organization's culture in an impartial manner before making comparisons with international norms and expectations. Guidance provided here, describing good practices, represents expert opinion but does not constitute recommendations made on the basis of a consensus of IAEA Member States.

This Safety Report is intended for use by senior management, safety culture specialists and employees working to assess and thereby strengthen the safety culture of:

- Nuclear facilities;
- Activities using sources of ionizing radiation;
- Radioactive waste management;
- The transport of radioactive material;
- Radiation protection activities;
- Any other practices or circumstances in which people may be exposed to radiation from naturally occurring or artificial sources.

This Safety Report can also be used for safety culture self-assessments of regulatory bodies which conduct oversight of the above mentioned activities. The Safety Report further applies to technical support organizations and vendors as well as other high reliability organizations.

The publication is applicable throughout the lifetime of facilities. For a facility, this usually includes the following phases: siting, design, construction, commissioning, operation and decommissioning (or close-out or closure).

Section 2 provides background information on the understanding of safety culture. Section 3 explores the purpose of SCSAs and the particular role of self-assessments. Section 4 describes generic process steps for conducting an SCSA. Section 5 describes the use of specific methods: document reviews, questionnaires, interviews, observations and focus groups. Each method is explored in terms of the process, advantages, limitations and risks, and potential uses. Section 6 provides guidance on how to work with the information from each method to perform an integrated analysis. Section 7 describes approaches to communicating the findings and transitioning hi to action.

Appendices I-IX provide additional guidance on the application of the methods in Section 5, as well as the research and theoretical base for this methodology. A theoretical supplement is provided in the Annex.